

pubs.acs.org/acssensors Article

## In Situ Spatiotemporal SERS Measurements and Multivariate Analysis of Virally Infected Bacterial Biofilms Using Nanolaminated Plasmonic Crystals

Aditya Garg, Wonil Nam, Wei Wang, Peter Vikesland,\* and Wei Zhou\*



Cite This: ACS Sens. 2023, 8, 1132-1142



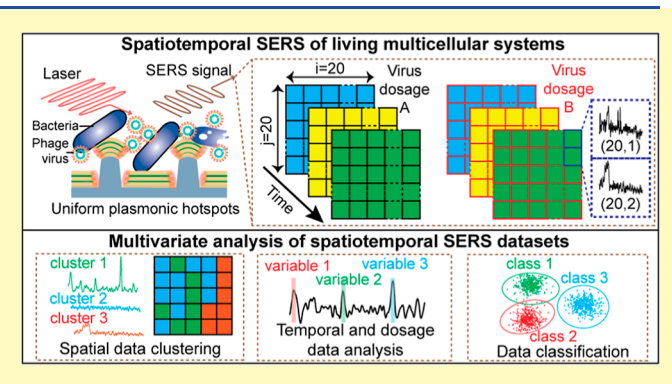
**ACCESS** I

Metrics & More

Article Recommendations

Supporting Information

ABSTRACT: In situ spatiotemporal biochemical characterization of the activity of living multicellular biofilms under external stimuli remains a significant challenge. Surface-enhanced Raman spectroscopy (SERS), combining the molecular fingerprint specificity of vibrational spectroscopy with the hotspot sensitivity of plasmonic nanostructures, has emerged as a promising noninvasive bioanalysis technique for living systems. However, most SERS devices do not allow reliable long-term spatiotemporal SERS measurements of multicellular systems because of challenges in producing spatially uniform and mechanically stable SERS hotspot arrays to interface with large cellular networks. Furthermore, very few studies have been conducted for multivariable analysis of spatiotemporal SERS datasets to extract spatially and temporally correlated biological



information from multicellular systems. Here, we demonstrate in situ label-free spatiotemporal SERS measurements and multivariate analysis of *Pseudomonas syringae* biofilms during development and upon infection by bacteriophage virus Phi6 by employing nanolaminate plasmonic crystal SERS devices to interface mechanically stable, uniform, and spatially dense hotspot arrays with the *P. syringae* biofilms. We exploited unsupervised multivariate machine learning methods, including principal component analysis (PCA) and hierarchical cluster analysis (HCA), to resolve the spatiotemporal evolution and Phi6 dose-dependent changes of major Raman peaks originating from biochemical components in *P. syringae* biofilms, including cellular components, extracellular polymeric substances (EPS), metabolite molecules, and cell lysate-enriched extracellular media. We then employed supervised multivariate analysis using linear discriminant analysis (LDA) for the multiclass classification of Phi6 dose-dependent biofilm responses, demonstrating the potential for viral infection diagnosis. We envision extending the in situ spatiotemporal SERS method to monitor dynamic, heterogeneous interactions between viruses and bacterial networks for applications such as phage-based anti-biofilm therapy development and continuous pathogenic virus detection.

KEYWORDS: surface-enhanced Raman spectroscopy, spatiotemporal SERS, bacterial biofilms, virus detection, multivariate analysis

## INTRODUCTION

Biofilms consist of microbial communities embedded in an extracellular polymeric substance (EPS) matrix<sup>1,2</sup> and feature spatially and temporally heterogeneous structures and compositions.<sup>2</sup> The introduction of external stimuli (e.g., antibiotics, viruses, and environmental changes in temperature, pH, or nutrients) can affect biofilm evolution by altering bacterial growth dynamics,<sup>3</sup> metabolic activity,<sup>4</sup> and cell-to-cell quorum sensing.<sup>5</sup> In situ spatiotemporal biochemical monitoring of biofilm activity remains an unmet challenge, causing the lack of a holistic system-level understanding of biofilm activity in response to external stimuli and impeding the development of anti-biofilm treatment methods (e.g., antibiotic and phage therapy).6 Furthermore, biofilms can potentially serve as living biosensor elements for detecting bioenvironmental stressors (e.g., viruses and metals) by reporting changes in spatiotemporal biofilm activity following stressor introduction. For

example, since bacteriophage viruses can alter host bacterial metabolism in favor of viral replication, it is possible to develop continuous virus detection methods by continuously monitoring bacterial metabolism changes in response to viral infection.  $^{4,7-9}$ 

Standard bioanalysis methods, including label-free mass spectrometry (MS),<sup>4,8</sup> nuclear magnetic resonance (NMR) spectroscopy,<sup>9</sup> and label-based fluorescence microscopy,<sup>10</sup> have been exploited to study bacterial responses to phage

Received: November 6, 2022 Accepted: February 27, 2023 Published: March 9, 2023





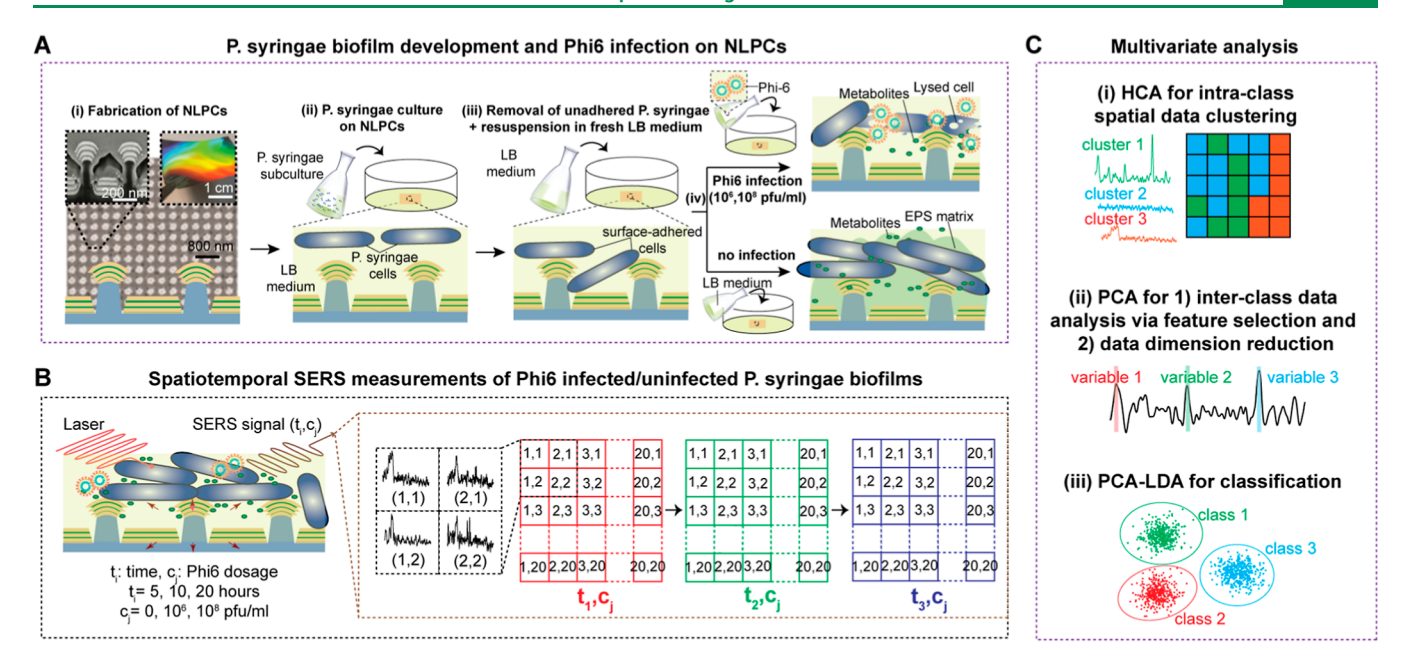


Figure 1. Key steps to achieve spatiotemporal SERS measurements and multivariate analysis of the growth processes and viral infection responses in bacterial biofilms. (A) Schematic illustrations of the biofilm development and viral infection processes on the NLPCs, including (i) fabrication of the NLPCs (camera image, top-down scanning electron microscope (SEM) image, and cross-sectional SEM image of the NLPCs are illustrated), (ii) bacteria culturing on the NLPCs, (iii) removal of unadhered cells, resuspension in fresh LB medium and Phi6 viral infection, and (iv) biofilm development on the NLPCs in uninfected and virally infected samples. (B) Schematic illustration of the methodology of spatiotemporal SERS measurements of living biofilms at times  $(t_i)$  with different Phi6 dosages  $(c_j)$ . (C) Schematic illustration of the unsupervised and supervised machine learning methods for multivariate analysis of multidimensional spatiotemporal SERS datasets, including (i) HCA for intra-class spatial data clustering, (ii) PCA for inter-class data analysis via feature selection and data dimension reduction, and (iii) PCA-LDA for SERS data classification.

infection or antibiotic treatment. However, these standard bioanalysis approaches cannot provide spatiotemporal bioanalysis of living biosystems due to their invasive nature. Recently, label-free surface-enhanced Raman spectroscopy (SERS), combining the molecular fingerprint specificity of vibrational spectroscopy with the hotspot sensitivity of plasmonic nanostructures, has emerged as an ultrasensitive, noninvasive molecular detection approach for in situ biochemical analysis of living systems. 11,12 Compared to standard Raman spectroscopy, SERS can minimize invasiveness and improve the throughput and reliability of in situ spatiotemporal measurements of living biosystems using a low laser power with a short acquisition time. 13

However, prior in situ SERS microbial studies have primarily focused on pathogen identification and antibiotic susceptibility testing using isolated individual bacterial cells. 14,15 Despite the utility of monitoring average population responses, SERS measurements of isolated individual bacterial cells cannot resolve dynamic heterogeneous bacterial activities in complex biofilm networks. Among the limited number of in situ SERS biofilm studies published to date, the majority have relied upon the incubation of biofilms with discrete colloidal plasmonic nanoparticle suspensions to detect molecular signatures (e.g., DNA, proteins, lipids, and carbohydrates) at the biofilm surface. <sup>13,16–18</sup> Unfortunately, in situ SERS measurements with discrete colloidal plasmonic nanoparticles face inherent challenges in allowing spatiotemporal monitoring of biofilms due to uncontrolled nanoparticle distribution, aggregation, and diffusion. In contrast, substrate-bound SERS devices can support dense and mechanically stable plasmonic hotspot arrays, 12,19,20 allowing reliable in situ spatiotemporal SERS measurements of multicellular systems. Recent studies have interfaced bacterial biofilms with substrate-bound SERS

devices covered with a nanoporous layer (e.g., mesoporous silica) to conduct 2D SERS measurements of the spatial distribution of quorum-sensing molecules (e.g., pyocyanin) secreted by bacterial cells in biofilms. Notably, the nanoporous layer on the SERS substrates can serve as a filter to block large biomolecules (e.g., proteins) from accessing plasmonic hotspots and thus allow higher signal-to-noise detection of small quorum-sensing molecules. However, such nanoporous layer-covered SERS devices inhibit holistic SERS profiling of various molecules associated with biofilm activity. Finally, substrate-bound SERS devices can integrate with microfluidic systems to monitor biofilm effluent media or precursor materials associated with biofilm responses, but such methods still have limitations in resolving spatiotemporal biofilm activities.

Due to challenges in low-cost nanofabrication of large-area, high-performance SERS devices with good biocompatibility for interfacing with living cellular networks, there has been little research on in situ spatiotemporal label-free SERS measurements and multivariate analysis of holistic molecular profiles associated with living multicellular systems. Since label-free SERS spectra measured from living biological systems consist of highly overlapped vibrational features from various biomolecules in plasmonic hotspots, we need to employ unsupervised or supervised machine learning methods to conduct multivariate analysis of high-dimensional SERS datasets for extracting biologically meaningful information.<sup>2</sup> Among unsupervised learning methods, principal component analysis (PCA) and hierarchical cluster analysis (HCA) are popular tools to extract interclass and intraclass relationships from intrinsic spectral features of sample groups (e.g., growth stages, cell types, disease/drug states) and reduce data dimensionality.<sup>28</sup> Supervised learning methods, such as linear

discriminant analysis (LDA) and support vector machines (SVM), can exploit the label information to train models for multivariate mapping to classify complex spectral features associated with different sample groups. <sup>29</sup> Despite advances in SERS bioanalysis of living cells, implementation of machine learning methods for multivariate analysis of spatiotemporal SERS datasets from living multicellular networks remains an underexplored topic.

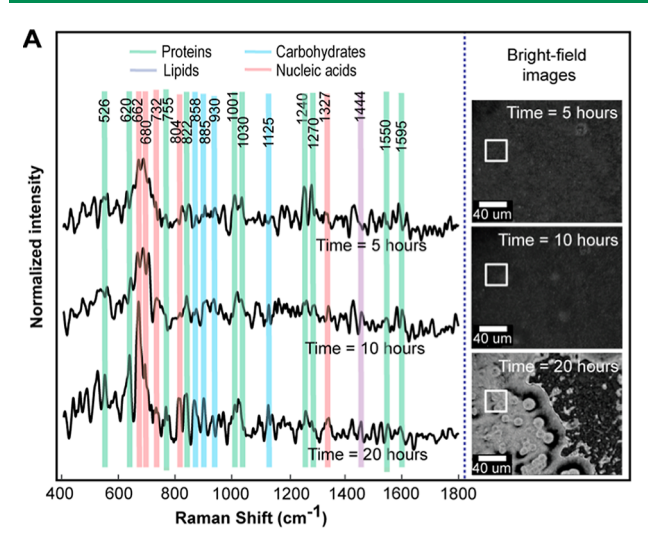
Here, we employ novel Au-SiO2-Au nanolaminated plasmonic crystals (NLPCs) to conduct in situ spatiotemporal label-free SERS measurements and multivariate analysis of Pseudomonas syringae biofilms during biofilm development and upon infection by bacteriophage virus Phi6 at different dosages. Significantly, we have combined multiple unsupervised and supervised machine learning methods to extract spatially and temporally correlated biological information from multivariable spatiotemporal SERS datasets measured from living biofilms. The lytic bacteriophage Phi6 is a recognized surrogate for enveloped infectious viruses such as SARS-CoV-2 and influenza virus, <sup>30,31</sup> and its host bacterium *P. syringae* is a representative human-safe biofilm-forming bacterium. 32,33 Accordingly, the P. syringae-Phi6 pair is a suitable humansafe model biosystem for our proof-of-concept studies. Our results are readily translatable to other biofilm-virus interactions for applications, including anti-biofilm phage therapy development and biofilm-enabled pathogenic virus detection.

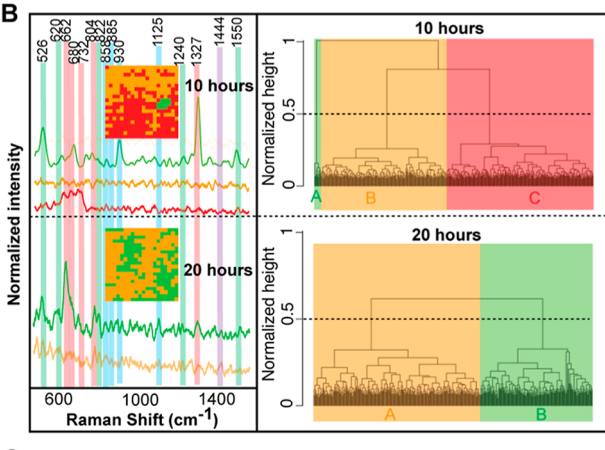
#### RESULTS AND DISCUSSION

Overall Experimental Workflow of Sample Preparation, Spatiotemporal SERS Measurements, and Multivariate Analysis. Figure 1 summarizes our approach in spatiotemporal SERS measurements and multivariate analysis of the P. syringae biofilm growth processes and the biofilm viral infection responses: (A) P. syringae biofilm development and Phi6 infection on the NLPCs, (B) in situ spatiotemporal SERS measurements of Phi6 infected/uninfected P. syringae biofilms, and (C) multivariate analysis by unsupervised and supervised machine learning methods. Our NLPC-based SERS samples consist of chemically inert and biocompatible Au-SiO<sub>2</sub>-Au multi-nanogap nanocavities to support mechanically stable, optically dense, highly uniform plasmonic hotspot arrays with SERS enhancement factors (EFs) >  $10^7$  [Figure 1A(i)]. P. syringae bacterial culture suspended in fresh lysogeny broth (LB) medium was pipetted onto the NLPCs to allow cell adherence to the SERS substrate. Following the removal of planktonic bacterial cells and the addition of fresh LB broth, bacterial biofilms developed on the NLPCs under external stimuli by different dosages of Phi6 bacteriophage (0, 10<sup>6</sup>, and 10<sup>8</sup> PFU/mL) [Figure 1A(ii-iv)]. Biofilm evolution consists of numerous spatiotemporally coupled biochemical processes (e.g., metabolic activity, EPS formation, quorum sensing). Bacteriophages can infect and replicate within the host bacteria, thus altering the local spatiotemporal biochemistry.<sup>4,8</sup> Spatiotemporally resolved label-free SERS measurements were acquired to monitor dynamic heterogeneous biofilm activities with and without viral infection (Figure 1B). The spatiotemporal SERS dataset consists of 400 data points measured over and 20 h) for three different Phi6 dosages ( $c_i = 0$ ,  $10^6$ , and  $10^8$ PFU/mL). To analyze and classify the complex multivariable SERS data consisting of 3600 data points from three different times and three Phi6 dosages, we employed unsupervised

(HCA and PCA) and supervised (PCA-LDA) machine learning methods (Figure 1C). Unsupervised HCA was employed to cluster the intra-class spatial data with Raman mode analysis [Figure 1C(i)]. Unsupervised PCA was used to analyze the inter-class data ( $t_i$  and  $c_j$ ) by identifying key spectral features responsible for inter-class variations. Furthermore, we exploited PCA as a data reduction tool for subsequent supervised machine learning analysis [Figure 1C(ii)]. For the supervised machine learning analysis, PCA-LDA was used to classify SERS spectra associated with the growth and phage dosage-dependent response of the *P. syringae* biofilms [Figure 1C(iii)].

Spatiotemporal SERS and Multivariate Spatial Data Analysis of the Biofilm Development Process. P. syringae biofilms were developed on the NLPCs, and a Raman microscope with a backscattering configuration was used to capture spatiotemporally correlated label-free SERS spectra of the developing biofilm. Compared to colloidal SERS probes, our NLPCs<sup>11</sup> can support mechanically stable, uniform, and dense plasmonic hotspot arrays for reliable spatiotemporal SERS measurements of living cellular networks. The NLPC SERS devices support healthy biofilm development, as indicated by the increased number of surface-adhered bacteria over time (Figure S1). Figure 2A shows average Raman spectra measured from a 400  $\mu$ m<sup>2</sup> region under 785 nm excitation following 5, 10, or 20 h of biofilm development, along with the corresponding bright field images. We calibrated the SERS signal intensities for each measurement using the electronic Raman scattering (ERS) internal standard.<sup>34</sup> This calibration can eliminate the effects of spatial and temporal variations of the local field intensity at the SERS hotspots caused by the spatiotemporally heterogeneous growth of biofilms on top of the SERS substrates, enabling accurate quantitative analysis. 12,34 To ensure a high signal-to-noise ratio, spectra whose maximum peak values were smaller than three times the noise level were discarded.<sup>35</sup> Figure S2 shows the noise level in the averaged SERS spectra of P. syringae biofilms at 20 h, indicating that the major SERS peaks from the P. syringae biofilm components have a higher signal intensity than the noise level. Table S1 summarizes the assigned origins of the observed SERS peaks. As shown in Figure 2A, several peaks attributed to proteins, carbohydrates, lipids, and nucleic acids emerge between 5 and 20 h of biofilm development (Text S1 in the Supporting Information). The development of these peaks reflects biofilm evolution-induced changes originating from the production of bacterial extracellular metabolites, <sup>24,36</sup> cell wall components,<sup>37</sup> and the EPS matrix.<sup>38</sup> However, the average label-free SERS spectra of P. syringae at different growth stages consist of highly overlapped and complex spectroscopic features. The highly overlapped and complex nature of the spectroscopic features can be attributed to the rich biomolecular composition of the living biological system, causing each data point to contain several spectroscopic features that arise from various biomolecules in SERS hotspots within the area illuminated by the Raman laser. Furthermore, the spatially heterogeneous distribution of biochemical components within the biofilm<sup>39</sup> causes significant point-to-point variations in the spectral profile over the measured region, generating highly overlapped features in the averaged spectra. Therefore, it is critical to employ multivariate machine learning methods to predict the origins of the observed SERS peaks and better understand the spatiotemporal biochemical evolution of the *P. syringae* biofilm.





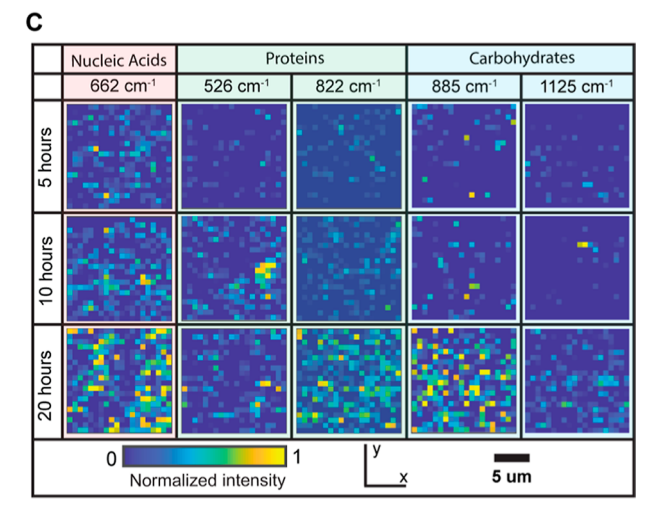


**Figure 2.** Spatiotemporal SERS measurements and intra-class multivariate analysis of the *P. syringae* biofilm development processes. (A) Average ERS-calibrated SERS spectra from the cultured *P. syringae* biofilm on the NLPCs at 5, 10, and 20 h, along with the corresponding bright-field images. Note: green lines, red lines, blue lines, and purple lines mark the known positions of the protein peaks, nucleic acid peaks, carbohydrate peaks, and lipid peaks, respectively. (B) HCA-extracted SERS spectra with color code, 2D HCA maps based on the corresponding HCA spectral color code, and HCA dendrograms of the spatiotemporal dataset from *P. syringae* biofilms at 10 and 20 h. (C) ERS-calibrated 2D SERS maps at 662, 526, 822, 885, and 1125 cm<sup>-1</sup> from *P. syringae* biofilms at 5, 10, and 20 h.

We employed HCA to resolve the time-dependent spatial SERS information hidden within the average SERS spectra (Figure 2B). By quantifying similarity distances between observations, HCA groups data points with similar spectral profiles, which allows visualization of the spatial distributions of various components in the biological matrix (e.g., cell wall, EPS, extracellular metabolites, and background culture medium). At t = 5 h, the clusters obtained via HCA demonstrate similar spectral profiles, indicating the uniform distribution of several significant biochemical components (Figure S3 in the Supporting Information). At t = 10 h, the HCA dendrogram reveals three clusters with a significant difference between cluster A (green) and the other two. Cluster A exhibits strong SERS peaks from proteins (526, 1240, and 1550 cm<sup>-1</sup>), carbohydrates (858 cm<sup>-1</sup>), and nucleic acids (1327 cm<sup>-1</sup>) originating from cell wall components intimately interfaced with the SERS hotspots on the NLPCs (Figure 2B). For validating the origins of these peaks, we conducted control experiments to obtain the SERS spectra of washed P. syringae cells suspended in phosphate-buffered saline (PBS) (Figure S4 in the Supporting Information). The spectrum of P. syringae cells measured immediately after washing with PBS solution also exhibited strong peaks at 526, 858, 1240, 1327, and 1550 cm<sup>-1</sup> (Figure S4 in the Supporting Information), indicating that these peaks originate from bacterial cell wall components. Additionally, we observed a peak at 930 cm<sup>-1</sup> in cluser A (C-O stretch/C-O-C vibration) associated with alginate, 40 which is a well-studied EPS matrix polysaccharide in *P. syringae* biofilms, <sup>41</sup> indicating the onset of EPS polysaccharide generation near the P. syringae cells at 10 h. The HCA-resolved spectrum from cluster B (orange) shows weak SERS signals, while the spectrum from cluster C (red) shows a strong SERS peak at 732 cm<sup>-1</sup> originating from the LB medium (Figure S5 in the Supporting Information). This result indicates the local consumption of LB medium components close to the SERS hotspots by the *P*. syringae cells in cluster B. However, the absence of SERS signals from cell wall components indicates a less intimate nano-bio interface between the cells and the plasmonic hotspots in cluster B at 10 h.

At t = 20 h, the HCA dendrogram reveals two clusters with considerable dissimilarity. The HCA-resolved spectrum for cluster A (orange) exhibits weak SERS signals that reflect the consumption of background LB medium components. The HCA-resolved SERS spectra and spatial maps reveal that cluster B (green) exhibits a rich spectral profile, covering a large surface area, indicating expansion of the bacterial biofilm network interfaced with the SERS hotspots. Apart from the peaks at 526, 858, 1240, 1327, and 1550 cm<sup>-1</sup> attributed to the cell wall components, we observed additional peaks originating from polysaccharides (885 and 1125 cm<sup>-1</sup>), <sup>40,42</sup> proteins (620 and 822 cm<sup>-1</sup>), and nucleic acids (804 cm<sup>-1</sup>) in the cluster B dataset, which can be attributed to the EPS of P. syringae biofilms (Figure 2B). 43 Lastly, a strong peak at 662 cm<sup>-1</sup> from guanine is observed in the cluster B dataset. Since the peak at 662 cm<sup>-1</sup> significantly increases in intensity between 0 and 12 h in the control SERS spectra of washed P. syringae cells under nutrient-deprived conditions (Figure S4), the feature at 662 cm<sup>-1</sup> likely originates from purine degradation metabolites at the SERS hotspots due to the starvation response of bacterial cells, as reported in prior studies. 44 Therefore, HCA analysis of the multidimensional SERS dataset enabled us to visualize the spatiotemporally correlated evolution of biochemical compo-

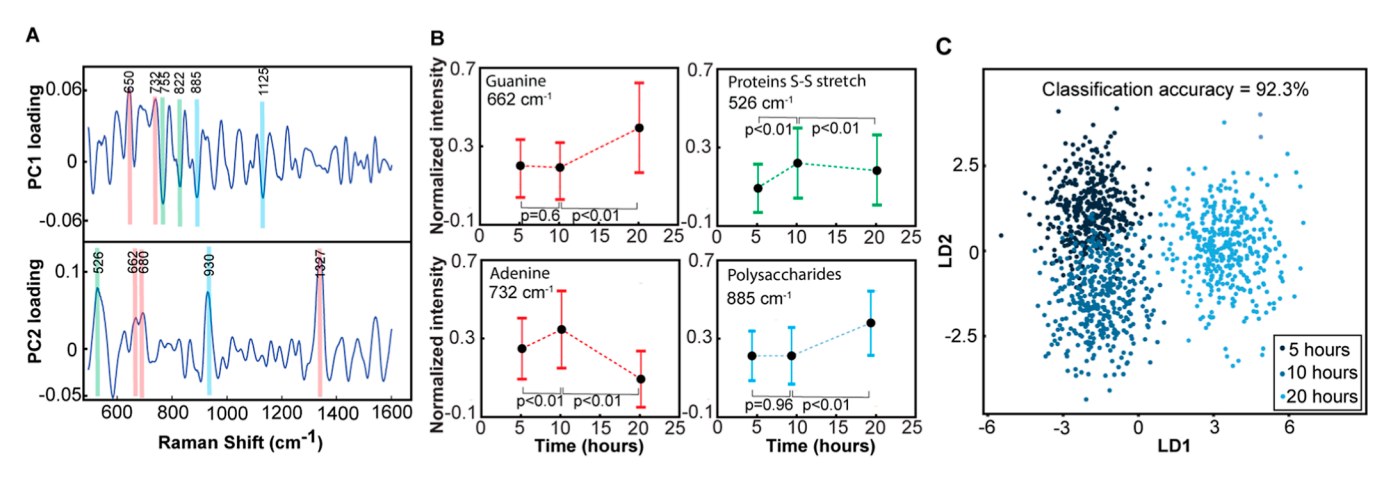


**Figure 3.** Inter-class multivariate analysis and classification of the spatiotemporal SERS datasets from *P. syringae* biofilms at different growth stages. (A) PC1 and PC2 loading spectra from the PCA analysis of SERS spectra from *P. syringae* biofilms at different growth times at 5, 10, and 20 h. (B) ERS-calibrated Raman intensities at 662, 732, 526, and 885 from *P. syringae* biofilms at 5, 10, and 20 h. (C) PCA-LDA score scatter plots for PCA-LDA with LOOCV from *P. syringae* biofilms at different growth times.

nents in living *P. syringae* biofilms, including cellular components, EPS matrix components, and metabolite molecules. To visualize the spatiotemporal biochemical changes of individual biomarkers during the biofilm growth process, we plotted 2D maps of the ERS-calibrated Raman intensities of major peaks from proteins, carbohydrates, and nucleic acids as a function of time (Figure 2C). Although the HCA analysis can extract the overall trend of the spatiotemporal biochemical evolution of the *P. syringae* biofilm, the non-uniform and dynamically changing spatial distributions of individual Raman peaks in Figure 2C reflect the heterogeneous structure and complex spatiotemporal evolution of the *P. syringae* biofilm.

Multivariate Analysis and Classification of the Growth Stages of *P. syringae* Biofilms. For the interclass temporal analysis of the multivariable SERS data from the *P. syringae* biofilm, we implemented PCA. As an unsupervised multivariate analysis method capable of extracting features with the highest variance, PCA is useful for extracting the inter-class spectral variations associated with different data classes (e.g., biofilm growth times and phage infection dosages) (Text S2 in Supporting Information). Figure 3A illustrates the loading spectra for the first two principal components of the SERS dataset of *P. syringae* biofilms at different times, revealing that different loadings consist of various spectral features with different molecular origins (Text S3 in the Supporting Information).

To investigate the temporal evolution of the individual spectral features identified by the principal component (PC) loading scores, we plotted the ERS-calibrated Raman intensities of the identified Raman features as a function of time (Figure 3B). First, we observe that the peak at 662 cm<sup>-1</sup> from purine metabolites significantly increases in intensity between 10 and 20 h. Concurrently, the peak from the LB medium (732 cm<sup>-1</sup>) significantly decreased between 10 and 20 h, reflecting the synergy between nutrient consumption and the release of purine degradation extracellular metabolites. Concurrently, rapid bacterial growth was also observed between 10 and 20 h (Figure S6 in the Supporting Information). Second, the peak intensity at 526 cm<sup>-1</sup>, attributed to the cell wall components, first increases from 5 to 10 h and subsequently decreases from 10 to 20 h. Concurrently, the intensities of peaks attributed to EPS

components at 822, 885, and 1125 cm<sup>-1</sup> rapidly increase between 10 and 20 h (Figures 3B and S7 in the Supporting Information). These observations indicate that the EPS components surround the cells as the *P. syringae* biofilm develops between 10 and 20 h with limited access of the cell wall components to the SERS hotspots. Although the normalized intensity of individual spectral features can allow us to understand the temporal trends of various biomolecules, they are insufficient to classify SERS spectra measured from different biofilm growth stages due to the intrinsically heterogeneous nature of biochemical environments in biofilms mapped by SERS hotspot arrays.

We employed supervised PCA-LDA methods to classify the measured SERS spectra acquired during different biofilm growth stages (Text S4 and Figure S8 in the Supporting Information). The first 75 PCs (95% spectral variance) were used as input variables for LDA to avoid overfitting. To use LDA, the number of input variables (75 PCs) should be at least 5 times lower than the number of spectra (1200 spectra). 45 The classification results demonstrate that the PCA-LDA model can achieve an overall classification accuracy of 92.3% (Figures 3C and S8B,C in the Supporting Information). We would like to point out that the LDA classification accuracy was 87.1% with the first five PCs as input variables. The next 70 PCs account for an additional 5.2% cumulative accuracy, which might originate from convoluted noise and real spectroscopic features due to the weak signal intensity of some SERS features. In sum, we can exploit unsupervised HCA and PCA methods to extract the spatial and temporal SERS information related to different biochemical components in biofilms and employ supervised PCA-LDA methods to classify SERS spectra associated with different biofilm growth stages. Compared to previous studies focused on label-free monitoring of either the spatial distribution or temporal evolution of biofilms, 17,38 this work is among the first to demonstrate spatiotemporal SERS measurements and multivariate analysis of the dynamic heterogeneous evolution of various molecules in living biofilms, including cellular components, EPS matrix components (e.g., polysaccharide alginate, proteins, and extracellular DNA), and metabolite molecules. Spatiotemporal SERS analysis of living biofilms can potentially aid the development of antibiofilm therapy methods by improving our understanding of the system-level response of virulent biofilms to therapeutic agents (e.g., bacteriophage viruses) such as different survival mechanisms (e.g., cell to cell quorum sensing, <sup>46</sup> polymicrobial synergy, <sup>47</sup> metabolic aspects <sup>48</sup>) and their interactions with each other.

Spatiotemporal SERS Profiling and Multivariate Spatial Data Analysis of Virally Infected Biofilms. As shown in Figure 4A, Phi6 can infect and replicate within P.

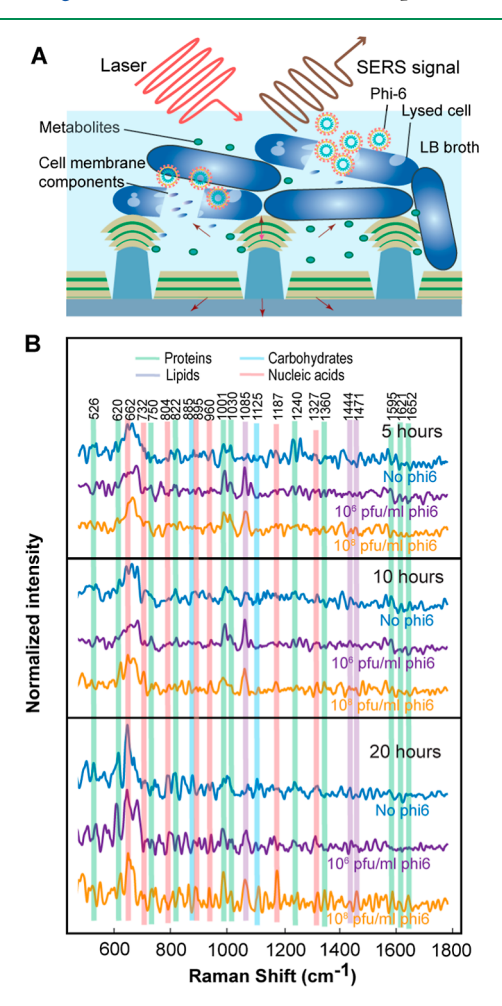


**Figure 4.** Spatiotemporal SERS measurements of *P. syringae* biofilms under Phi6 viral infection at different dosages. (A) Schematic illustration of the experimental setup. (B) Average SERS spectra from *P. syringae* biofilms without viral infection (blue) and with Phi6 viral infection at two dosages of 10<sup>6</sup> PFU/mL (purple) and 10<sup>8</sup> PFU/mL (orange) at 20 h. Note: green lines, red lines, blue lines, and purple lines mark the known positions of the protein peaks, nucleic acid peaks, carbohydrate peaks, and lipid peaks, respectively.

syringae cells and thereby alter the spatiotemporal biochemical information at the SERS hotspots due to a range of mechanisms such as the disruption of biofilm integrity by the lytic action of Phi6, 50 the buildup of molecular components from lysed cells in the extracellular environment, and the alteration of host bacterial metabolism in favor of viral replication. We performed in situ spatiotemporal SERS measurements of biofilm development under Phi6 viral infection at dosages of 0, 106, and 108 PFU/mL to study dose effects on *P. syringae* biofilm activity. As expected, Phi6 infection can inhibit *P. syringae* growth due to the lytic action of Phi6 (Figure S6 in the Supporting Information). Figure 4B

shows the ERS-normalized average SERS spectra measured at 5, 10, and 20 h over a 400  $\mu$ m<sup>2</sup> region of the virally infected (10<sup>6</sup> and 10<sup>8</sup> PFU/mL Phi6) and uninfected living biofilms on the NLPCs. At t = 5 h, the observed SERS spectra of virally infected samples exhibit an additional peak at 1085 cm<sup>-1</sup>, attributed to membrane phospholipids. At t = 10 h, peaks at 960 and 1187 cm<sup>-1</sup>, attributed to nucleic acids, are observed in the SERS spectra of samples infected with 10<sup>8</sup> PFU/mL Phi6. At t = 20 h, several peaks originating from proteins at 750, 1360, and 1621 cm<sup>-1</sup> (tryptophan) and 1652 cm<sup>-1</sup> (amide I) emerge in the SERS spectra of samples infected with 108 PFU/ mL Phi6, while the peaks from phenylalanine (1001 and 1595 cm<sup>-1</sup>) significantly increase in intensity. Since a weak SERS signature was observed during the direct label-free detection of Phi6 (Figure S9 in the Supporting Information), these peaks can originate from cellular components in the extracellular environment released from lysed P. syringae cells due to the lytic action of Phi6. Previous studies employing MS have similar observations that accumulated cellular materials from lysed bacterial cells in phage-infected supernatants can increase the concentrations of specific amino acids, lipids, and nucleic acids.<sup>8,52</sup> The improved SERS signal intensity of lysed cell components compared to intact bacterial cells can be attributed to the improved accessibility of the smaller lysed cell components in the extracellular medium to the nanoscale SERS hotspots.

Since intact bacterial cells in virally infected samples can remain active and consume molecular components from lysed bacterial cells for promoting viral replication, the detected molecules in the SERS spectra of the virally infected samples at different time points reflect the virus-specific alteration of the bacterial metabolism.<sup>4,8</sup> Since Phi6 consists of 62% protein,<sup>5</sup> we believe that the absence of the protein peaks after 5 and 10 h of infection can be attributed to the active P. syringae cells' preferential consumption of amino acids from lysed cells to promote Phi6 propagation, thus limiting their presence in the SERS hotspot-probed extracellular environment. As the ratio of the active P. syringae cells to Phi6 particles decreases with time due to rapid Phi6 replication and the lytic action of Phi6, amino acids can likely buildup in the extracellular environment at later times, as indicated by the emergence of amino acidrelated SERS peaks at 20 h. In comparison, the phospholipid and nucleic acid components from lysed cells begin to build up in the SERS hotspot-probed extracellular environment within 5 and 10 h, respectively. Previous studies using MS<sup>8</sup> and NMR<sup>9</sup> have also demonstrated the preferential consumption of amino acids over lipid components by phage-infected bacteria from the cell lysate-enriched extracellular environment at early stages of infection for promoting the propagation of proteinrich bacteriophage viruses.

To visualize the embedded spatial information, we plotted the spatial maps of the HCA-resolved spectra and the ERS-calibrated Raman intensities of major peaks from infected and uninfected biofilms at 20 h (Text S5, Figures S10 and S11). The uninfected biofilms demonstrate spatially correlated spectroscopic signatures corresponding to biofilm components, indicating the development of *P. syringae* biofilms intimately interfaced with the SERS hotspots of the NLPCs (Figures 2B,C and S11A, Text S5 in the Supporting Information). In contrast, the infected biofilms demonstrate the non-uniform and spatially uncorrelated distribution of biomolecules from lysed cell components indicating the random adsorption—desorption at plasmonic nanogap cavities for different

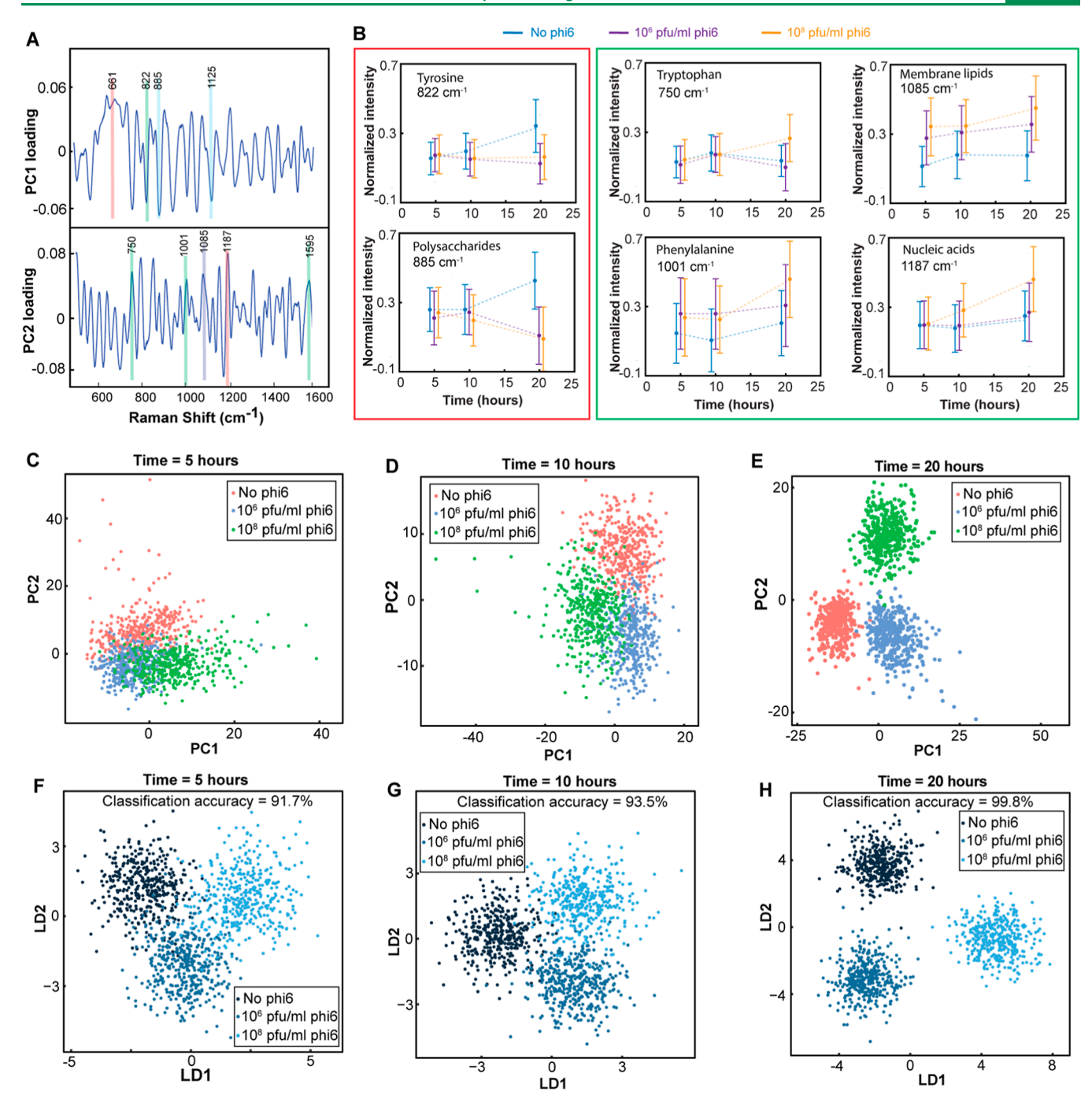


**Figure 5.** Inter-class multivariate analysis and classification of the spatiotemporal SERS datasets from *P. syringae* biofilms at different Phi6 viral infection dosages. (A) PC1 and PC2 loading spectra for the measured SERS spectra from *P. syringae* biofilms without viral infection and with Phi6 viral infection at two dosages of  $10^6$  PFU/mL (purple) and  $10^8$  PFU/mL (orange) after 20 h (B) ERS-calibrated Raman intensities at 750, 822, 855, 1000, 1082, and 1177 cm<sup>-1</sup> of uninfected *P. syringae* (blue) and *P. syringae* infected by  $10^6$  PFU/mL (purple) and  $10^8$  PFU/mL (orange) of Phi6 after 5, 10, and 20 h (C–H) PC and PCA-LDA scatter plots from *P. syringae* biofilms without viral infection and with Phi6 viral infection at  $10^6$  PFU/mL and  $10^8$  PFU/mL after (C,F) 5 h, (D,G) 10 h, and (E,H) 20 h.

molecules from lysed cell components in the extracellular environments (Figure S11 and Text S5 in the Supporting Information). To validate our assumptions about the spatiotemporal evolution of the phage-infected and uninfected *P. syringae* biofilms on the NLPCs (Figure S12A in SI) and planktonic *P. syringae* cells in the supernatant (Figure S12B in the Supporting Information), we performed fluorescence imaging using SYBR Green 1 nucleic acid stain (Text S6 in Supporting Information). These results further support that

the SERS signals in uninfected samples predominantly originate from biofilm components, while the signals in phage-infected samples primarily originate from lysed cell components in the extracellular environment. We want to point out that compared to the invasive fluorescence imaging method, which provides the single-time point spatial distribution information using label-based biomarkers, our spatiotemporal SERS measurements with NLPCs can achieve

real-time longitudinal mapping of the evolution of molecular constituents in the biofilms.

Multivariate Analysis and Classification of the Phi6-Dosage Dependent Responses of *P. syringae* Biofilms. To analyze the phage-dosage-dependent responses of the *P. syringae* biofilm from the multivariate SERS dataset, we first implemented PCA to identify critical spectral features. Figure SA illustrates the loading spectra for the first two principal components from the SERS dataset of the uninfected and infected samples (10<sup>6</sup> and 10<sup>8</sup> PFU/mL of Phi6) at 20 h. The PC1-loading spectrum primarily consists of the peaks observed in the uninfected samples at 822, 885, and 1125 cm<sup>-1</sup> attributed to EPS components, while the PC2-loading spectrum primarily consists of peaks observed in the infected samples at 750, 1001, 1085, 1187, and 1595 cm<sup>-1</sup> attributed to lysed cell components.

To quantitatively analyze the temporal biochemical changes of individual biomarkers identified by the PC loading scores in infected and uninfected samples, the ERS-calibrated Raman intensities of the identified features were plotted as a function of time (Figure 5B). First, we observe that the intensities for peaks attributed to the biofilm EPS polysaccharides at 885 cm<sup>-1</sup> and EPS proteins at 822 cm<sup>-1</sup> increase with time from 5 to 20 h in the uninfected biofilms, while these peaks do not increase in intensity with time in the infected biofilms, suggesting disruption of biofilm formation due to bacterial cell lysis.<sup>\$4</sup> Second, we observe that the peaks attributed to cellular components released from lysed cells exhibit varying temporal trends in the infected and uninfected samples. The peak intensity of the lipid peak (1085 cm<sup>-1</sup>) is consistently higher in the infected samples compared to the uninfected samples between 5 and 20 h. The peak intensity of the nucleic acid peak (1187 cm<sup>-1</sup>) gradually increases between 5 and 20 h in samples infected with 108 PFU/mL, and the peak intensity of the protein peaks (750 and 1001 cm<sup>-1</sup>) rapidly increases between 10 and 20 h in samples infected with 10<sup>8</sup> PFU/mL. As mentioned earlier, the unique temporal trends of different macromolecules in the biological matrix of virally infected samples can reflect the virus-specific alteration of bacterial metabolism.<sup>4,8</sup> By extending our model to other virus-cell interactions, our methodology can potentially enable the continuous diagnosis of pathogenic viruses.

Although the average intensity of individual spectral features can allow us to understand the temporal trend of various biomolecules, they are insufficient to classify SERS spectra measured from virally infected and uninfected biofilm samples for viral diagnosis due to the intrinsically heterogeneous nature of the biochemical environments in biofilms mapped by SERS hotspot arrays. Therefore, we employed PCA-LDA to statistically classify the virus-infected and uninfected biofilms at different growth stages. In Figure 5C, the PC score plot with scatters from uninfected, low-dose infected, and high-dose infected biofilms after 5 h of development shows the extensive overlap between the low-dose infected and high-dose infected biofilms. A similar overlap pattern can be observed in the PC score plot after 10 h of biofilm development (Figure 5D). In contrast, at 20 h, the PC score plot shows a clear separation between the three cases (Figure 5E), manifesting significant differences in the spectra at later stages of biofilm development. Such behaviors are likely due to the viral-dosedependent accumulation of lysed cell components in the extracellular environment of the infected biofilm and the development of a robust biofilm EPS in the uninfected biofilm.

PCA was used as a data reduction tool to extract significant variables from the data set, and subsequently, LDA was implemented to classify the multivariable dataset at t=5, 10, and 20 h using the first 75 PC components as input variables. As shown in Figure 5F–H, the PCA-LDA classification model can effectively segregate the uninfected, low-dose infected, and high-dose infected biofilms at t=5, 10, and 20 h. The PCA-LDA classification results obtained using the leave-one-outcross-validation method indicate that overall accuracies of 91.7, 93.5, and 99.8% can be achieved at t=5, 10, and 20 h, respectively, validating the potential for viral infection diagnosis (Figure S13 in the Supporting Information).

### CONCLUSIONS

In conclusion, we have demonstrated that NLPCs, consisting of dense and uniformly distributed SERS hotspots, can enable reliable in situ spatiotemporal SERS measurements of living P. syringae biofilms to monitor the spatiotemporal evolution of the network-level microbial activity during the biofilm growth process. Using multivariate machine learning methods such as HCA and PCA, we have extracted spatially and temporally correlated biological information embedded in the multivariable spatiotemporal SERS datasets, demonstrating the spatial distribution and temporal evolution of important biomolecules related to cell wall components, EPS matrixes, and extracellular metabolites in the P. syringae biofilm matrix. Moreover, when infected by bacteriophage Phi6, the spatiotemporal biochemical changes in the biological matrix due to the phage-bacteria interaction were monitored, allowing reliable multiclass-classification analyses of the phage dosage-dependent responses of living P. syringae biofilms using supervised PCA-LDA machine learning methods. Our results indicate that the temporal dynamics of different biomolecules observed in the SERS spectra from lysed bacterial cell components, such as amino acids, nucleic acids, and lipids, can reflect the virus-specific alteration of the metabolism of host bacteria. Therefore, our developed methods can potentially extend to measure and analyze the spatiotemporal interactions between pathogenic viruses and various living multicellular systems consisting of mammalian cells or genetically engineered bacteria.<sup>36</sup> Moreover, we envision that the ability to capture, analyze, and differentiate the dynamically evolving spatiotemporal biochemical activities of living biofilms in response to external stimuli (e.g., temperature, antibiotics, and bacteriophages) can potentially assist in the development of effective anti-biofilm treatment methods.

### EXPERIMENTAL SECTION

Spatiotemporal SERS Analysis of Uninfected and Phi6-Infected *P. syringae*. NLPCs were attached to the bottom of sterile 60 mm Petri dishes using PU (UV curing for 3 min), and the system was sterilized with ethanol for 3 h. The prepared *P. syringae* suspension was washed with 10 mL of LB medium (3 times) and resuspended to a final concentration of  $10^7$  CFU/mL. 5 mL of the bacterial suspension was added to the system and incubated at 25 °C for 12 h to allow the *P. syringae* cells to adhere to the surface of the NLPCs. Then, we aspirated 5 mL of the solution in the Petri dish to remove the growth media and unadhered planktonic cells. We gently rinsed the adhered bacterial cells by adding 5 mL of fresh LB medium and aspirating the rinsing medium (2 times). Then, we added 4.9 mL of fresh LB medium to the Petri dishes. Lastly,  $100~\mu$ L of LB medium (uninfected case) and  $100~\mu$ L of Phi6 suspension with appropriate concentrations (infected cases) were added to the individual systems.

The three experiments (0,  $10^6$ , and  $10^8$  PFU/mL Phi6) were performed sequentially. SERS measurements were performed via a 20× objective lens with 2 mW power and 1s integration time over 20  $\mu$ m × 20  $\mu$ m regions containing 400 pixels at 5, 10, and 20 h for each case. Between SERS measurements, the Petri dishes remained in the same position to obtain spatially correlated data, and the Petri dishes were covered to prevent evaporation of the solution.

Multivariate Analysis. Baseline correction, Savitzky–Golay smoothing, and cosmic ray removal were performed using Project v4.1 software. Spectra whose maximum peak values were smaller than three times the noise level were discarded. The background noise intensity was determined using recorded background signals in the spectral region at 2000 cm<sup>-1</sup> without molecular Raman peaks.<sup>35</sup> MATLAB was used for performing ERS calibration and data truncation. Lastly, R was used for performing HCA, PCA, and LDA. For PCA and HCA, Raman wavenumbers from 500 to 1600 cm<sup>-1</sup> were chosen as variables. HCA was performed using Euclidian distance and Ward's minimum variance method. In the HCA dendrograms, a normalized distance threshold of 0.5 was used for assigning the clusters. Student's t-test was conducted using MATLAB, and the p-value describes the result of the t-test. p < 0.01 represents a significant difference.

## ASSOCIATED CONTENT

## Supporting Information

The Supporting Information is available free of charge at https://pubs.acs.org/doi/10.1021/acssensors.2c02412.

Additional experimental details; average SERS spectra of the *P. syringae* biofilm with the noise level; HCA analysis at 5 h; SERS spectra of washed *P. syringae* cells; SERS spectra of LB medium; *P. syringae* growth curves; PCA-LDA analysis of biofilm growth stages; SERS spectra of Phi6; HCA dendrograms of infected and uninfected samples at 20 h; spatial analysis of Phi6 infected biofilms; fluorescence microscopy images; confusion matrix for PCA-LDA of the viral-dose dependent responses of *P. syringae* biofilms; and assignments and origins for the observed SERS peaks (PDF)

## AUTHOR INFORMATION

#### **Corresponding Authors**

Peter Vikesland — Department of Civil and Environmental Engineering, Virginia Tech, Blacksburg, Virginia 24061, United States; orcid.org/0000-0003-2654-5132; Email: pvikes@vt.edu

Wei Zhou — Department of Electrical and Computer Engineering, Virginia Tech, Blacksburg, Virginia 24061, United States; ⊙ orcid.org/0000-0002-5257-3885; Email: wzh@vt.edu

#### **Authors**

Aditya Garg — Department of Electrical and Computer Engineering, Virginia Tech, Blacksburg, Virginia 24061, United States

Wonil Nam – Department of Electrical and Computer Engineering, Virginia Tech, Blacksburg, Virginia 24061, United States; Department of Electronic Engineering, Pukyong National University, Busan 48513, Republic of Korea; ⊚ orcid.org/0000-0002-7804-3049

Wei Wang — Department of Civil and Environmental Engineering, Virginia Tech, Blacksburg, Virginia 24061, United States; orcid.org/0000-0002-6231-2216

Complete contact information is available at: https://pubs.acs.org/10.1021/acssensors.2c02412

#### **Author Contributions**

The manuscript was written through the contributions of all authors. All authors have approved the final version of the manuscript.

#### Notes

The authors declare no competing financial interest.

#### ACKNOWLEDGMENTS

This work was supported by the US National Science Foundation grants OISE-1545756, CBET-2029911, and CBET-2231807 by AFOSR Young Investigator Award FA9550-18-1-0328 and by Wellcome Leap Inc (A5M3XP5X). Laboratory and instrumentation support was provided by NanoEarth—a node of the NSF-supported NNCI (NSF award number #1542100). Additional support was provided by the Sustainable Nanotechnology Interdisciplinary Graduate Program (VTSuN IGEP) funded by Virginia Tech.

#### REFERENCES

- (1) Flemming, H.-C.; Neu, T. R.; Wozniak, D. J. The EPS matrix: the "house of biofilm cells". *J. Bacteriol* **2007**, *189*, 7945–7947.
- (2) Flemming, H.-C.; Wingender, J. The biofilm matrix. *Nature reviews microbiology* **2010**, *8*, 623–633.
- (3) Toyofuku, M.; Inaba, T.; Kiyokawa, T.; Obana, N.; Yawata, Y.; Nomura, N. Environmental factors that shape biofilm formation. *Biosci., Biotechnol., Biochem.* **2016**, *80*, 7–12.
- (4) De Smet, J.; Zimmermann, M.; Kogadeeva, M.; Ceyssens, P.-J.; Vermaelen, W.; Blasdel, B.; Bin Jang, H.; Sauer, U.; Lavigne, R. High coverage metabolomics analysis reveals phage-specific alterations to Pseudomonas aeruginosa physiology during infection. *ISME j* **2016**, 10, 1823–1835.
- (5) Moreno-Gámez, S.; Sorg, R. A.; Domenech, A.; Kjos, M.; Weissing, F. J.; van Doorn, G. S.; Veening, J.-W. Quorum sensing integrates environmental cues, cell density and cell history to control bacterial competence. *Nat. Commun.* **2017**, *8*, 854.
- (6) Funari, R.; Shen, A. Q. Detection and Characterization of Bacterial Biofilms and Biofilm-Based Sensors. *ACS sensors* **2022**, 7, 347–357.
- (7) Chevallereau, A.; Blasdel, B. G.; De Smet, J.; Monot, M.; Zimmermann, M.; Kogadeeva, M.; Sauer, U.; Jorth, P.; Whiteley, M.; Debarbieux, L.; et al. Next-Generation "-omics" Approaches Reveal a Massive Alteration of Host RNA Metabolism during Bacteriophage Infection of Pseudomonas aeruginosa. *PLOS Genetics* **2016**, *12*, No. e1006134.
- (8) Ankrah, N. Y. D.; May, A. L.; Middleton, J. L.; Jones, D. R.; Hadden, M. K.; Gooding, J. R.; LeCleir, G. R.; Wilhelm, S. W.; Campagna, S. R.; Buchan, A. Phage infection of an environmentally relevant marine bacterium alters host metabolism and lysate composition. *ISME J* **2014**, *8*, 1089–1100.
- (9) Papaianni, M.; Cuomo, P.; Fulgione, A.; Albanese, D.; Gallo, M.; Paris, D.; Motta, A.; Iannelli, D.; Capparelli, R. Bacteriophages Promote Metabolic Changes in Bacteria Biofilm. *Microorganisms* **2020**, *8*, 480.
- (10) Yang, X.; Wisuthiphaet, N.; Young, G. M.; Nitin, N. Rapid detection of Escherichia coli using bacteriophage-induced lysis and image analysis. *PloS one* **2020**, *15*, No. e0233853.
- (11) Nam, W.; Ren, X.; Tali, S. A. S.; Ghassemi, P.; Kim, I.; Agah, M.; Zhou, W. Refractive-index-insensitive nanolaminated SERS substrates for label-free Raman profiling and classification of living cancer cells. *Nano letters* **2019**, *19*, 7273–7281.
- (12) Garg, A.; Mejia, E.; Nam, W.; Vikesland, P.; Zhou, W. Biomimetic Transparent Nanoplasmonic Meshes by Reverse-Nano-imprinting for Bio-Interfaced Spatiotemporal Multimodal SERS Bioanalysis. *Small* **2022**, *18*, 2204517.
- (13) Ivleva, N. P.; Wagner, M.; Horn, H.; Niessner, R.; Haisch, C. Raman microscopy and surface-enhanced Raman scattering (SERS) for in situ analysis of biofilms. *J. Biophotonics* **2010**, *3*, 548.

- (14) Premasiri, W.; Chen, Y.; Williamson, P.; Bandarage, D.; Pyles, C.; Ziegler, L. Rapid urinary tract infection diagnostics by surface-enhanced Raman spectroscopy (SERS): identification and antibiotic susceptibilities. *Anal. Bioanal. Chem.* **2017**, *409*, 3043–3054.
- (15) Walter, A.; März, A.; Schumacher, W.; Rösch, P.; Popp, J. Toward a fast, high specific and reliable discrimination of bacteria on strain level by means of SERS in a microfluidic device. *Lab Chip* **2011**, *11*, 1013–1021.
- (16) Chao, Y. Q.; Zhang, T. Surface-enhanced Raman scattering (SERS) revealing chemical variation during biofilm formation: from initial attachment to mature biofilm. *Anal. Bioanal. Chem.* **2012**, 404, 1465–1475.
- (17) Ivleva, N. P.; Wagner, M.; Szkola, A.; Horn, H.; Niessner, R.; Haisch, C. Label-free in situ SERS imaging of biofilms. *J. Phys. Chem. B* **2010**, *114*, 10184–10194.
- (18) Efeoglu, E.; Culha, M. In situ-monitoring of biofilm formation by using surface-enhanced Raman scattering. *Appl. Spectrosc.* **2013**, *67*, 498–505.
- (19) Garg, A.; Mejia, E.; Nam, W.; Nie, M.; Wang, W.; Vikesland, P.; Zhou, W. Microporous Multiresonant Plasmonic Meshes by Hierarchical Micro—Nanoimprinting for Bio-Interfaced SERS Imaging and Nonlinear Nano-Optics. *Small* 2022, *18*, 2106887.
- (20) Garg, A.; Nam, W.; Zhou, W. Reusable Surface-Enhanced Raman Spectroscopy Membranes and Textiles via Template-Assisted Self-Assembly and Micro/Nanoimprinting. ACS Appl. Mater. Interfaces 2020, 12, 56290–56299.
- (21) Bodelón, G.; Montes-García, V.; López-Puente, V.; Hill, E. H.; Hamon, C.; Sanz-Ortiz, M. N.; Rodal-Cedeira, S.; Costas, C.; Celiksoy, S.; Pérez-Juste, I.; et al. Detection and imaging of quorum sensing in Pseudomonas aeruginosa biofilm communities by surface-enhanced resonance Raman scattering. *Nat. Mater.* **2016**, *15*, 1203.
- (22) Bodelón, G.; Montes-García, V.; Costas, C.; Pérez-Juste, I.; Pérez-Juste, J.; Pastoriza-Santos, I.; Liz-Marzán, L. M. Imaging Bacterial Interspecies Chemical Interactions by Surface-Enhanced Raman Scattering. *Acs Nano* **2017**, *11*, 4631–4640.
- (23) Guo, J.; Liu, Y.; Chen, Y.; Li, J.; Ju, H. A multifunctional SERS sticky note for real-time quorum sensing tracing and inactivation of bacterial biofilms. *Chem. Sci.* **2018**, *9*, 5906–5911.
- (24) De Marchi, S.; García-Lojo, D.; Bodelón, G.; Pérez-Juste, J.; Pastoriza-Santos, I. Plasmonic Au@ Ag@ mSiO2 Nanorattles for In Situ Imaging of Bacterial Metabolism by Surface-Enhanced Raman Scattering Spectroscopy. ACS Appl. Mater. Interfaces 2021, 13, 61587–61597.
- (25) Nguyen, C. Q.; Thrift, W. J.; Bhattacharjee, A.; Ranjbar, S.; Gallagher, T.; Darvishzadeh-Varcheie, M.; Sanderson, R. N.; Capolino, F.; Whiteson, K.; Baldi, P.; Hochbaum, A. I.; Ragan, R. Longitudinal monitoring of biofilm formation via robust surfaceenhanced Raman scattering quantification of Pseudomonas aeruginosa-produced metabolites. ACS Appl. Mater. Interfaces 2018, 10, 12364–12373.
- (26) Paquet-Mercier, F.; Aznaveh, N. B.; Safdar, M.; Greener, J. A microfluidic bioreactor with in situ SERS imaging for the study of controlled flow patterns of biofilm precursor materials. *Sensors* **2013**, 13, 14714–14727.
- (27) Cui, F. Y.; Yue, Y.; Zhang, Y.; Zhang, Z. M.; Zhou, H. S. Advancing Biosensors with Machine Learning. *Acs Sensors* **2020**, *5*, 3346–3364.
- (28) Ringnér, M. What is principal component analysis? *Nat. Biotechnol.* **2008**, 26, 303–304.
- (29) Morais, C. L.; Lima, K. M.; Singh, M.; Martin, F. L. Tutorial: multivariate classification for vibrational spectroscopy in biological samples. *Nat. Protoc.* **2020**, *15*, 2143–2162.
- (30) Aquino de Carvalho, N.; Stachler, E. N.; Cimabue, N.; Bibby, K. Evaluation of Phi6 persistence and suitability as an enveloped virus surrogate. *Environ. Sci. Technol.* **2017**, *51*, 8692–8700.
- (31) Fedorenko, A.; Grinberg, M.; Orevi, T.; Kashtan, N. Survival of the enveloped bacteriophage Phi6 (a surrogate for SARS-CoV-2) in evaporated saliva microdroplets deposited on glass surfaces. *Scientific reports* **2020**, *10*, 22419.

- (32) Shao, X.; Xie, Y.; Zhang, Y.; Deng, X. Biofilm formation assay in Pseudomonas syringae. *Bio-protocol* **2019**, *9*, No. e3237.
- (33) Heredia-Ponce, Z.; Gutiérrez-Barranquero, J. A.; Purtschert-Montenegro, G.; Eberl, L.; Cazorla, F. M.; de Vicente, A. Biological role of EPS from Pseudomonas syringae pv. syringae UMAF0158 extracellular matrix, focusing on a Psl-like polysaccharide. *npj Biofilms and Microbiomes* **2020**, *6*, 37.
- (34) Nam, W.; Zhao, Y.; Song, J.; Ali Safiabadi Tali, S.; Kang, S.; Zhu, W.; Lezec, H. J.; Agrawal, A.; Vikesland, P. J.; Zhou, W. Plasmonic Electronic Raman Scattering as Internal Standard for Spatial and Temporal Calibration in Quantitative Surface-Enhanced Raman Spectroscopy. *J. Phys. Chem. Lett.* **2020**, *11*, 9543–9551.
- (35) Nam, W.; Chen, H.; Ren, X.; Agah, M.; Kim, I.; Zhou, W. Nanolaminate Plasmonic Substrates for High-Throughput Living Cell SERS Measurements and Artificial Neural Network Classification of Cellular Drug Responses. ACS Appl. Nano Mater. 2022, 5, 10358–10368.
- (36) Wang, W.; Kang, S.; Vikesland, P. J. Surface-Enhanced Raman Spectroscopy of Bacterial Metabolites for Bacterial Growth Monitoring and Diagnosis of Viral Infection; Environmental Science & Technology, 2021.
- (37) Liu, T.-T.; Lin, Y.-H.; Hung, C.-S.; Liu, T.-J.; Chen, Y.; Huang, Y.-C.; Tsai, T.-H.; Wang, H.-H.; Wang, D.-W.; Wang, J.-K.; Wang, Y.-L.; Lin, C.-H. A high speed detection platform based on surface-enhanced Raman scattering for monitoring antibiotic-induced chemical changes in bacteria cell wall. *PloS one* **2009**, *4*, No. e5470.
- (38) Chao, Y.; Zhang, T. Surface-enhanced Raman scattering (SERS) revealing chemical variation during biofilm formation: from initial attachment to mature biofilm. *Anal. Bioanal. Chem.* **2012**, *404*, 1465–1475.
- (39) Stewart, P. S.; Franklin, M. J. Physiological heterogeneity in biofilms. *Nat. Rev. Microbiol.* **2008**, *6*, 199–210.
- (40) Schmid, T.; Messmer, A.; Yeo, B.-S.; Zhang, W.; Zenobi, R. Toward chemical analysis of nanostructures in biofilms II: tipenhanced Raman spectroscopy of alginates. *Anal. Bioanal. Chem.* **2008**, 391, 1907–1916.
- (41) Preston, L. A.; Wong, T.; Bender, C. L.; Schiller, N. L. Characterization of alginate lyase from Pseudomonas syringae pv. syringae. *J. Bacteriol.* **2000**, *182*, 6268–6271.
- (42) Jung, G. B.; Nam, S. W.; Choi, S.; Lee, G.-J.; Park, H.-K. Evaluation of antibiotic effects on Pseudomonas aeruginosa biofilm using Raman spectroscopy and multivariate analysis. *Biomed. Opt. Express* **2014**, *5*, 3238–3251.
- (43) Mann, E. E.; Wozniak, D. J. Pseudomonas biofilm matrix composition and niche biology. *FEMS Microbiol. Rev.* **2012**, *36*, 893–916.
- (44) Premasiri, W. R.; Lee, J. C.; Sauer-Budge, A.; Théberge, R.; Costello, C. E.; Ziegler, L. D. The biochemical origins of the surface-enhanced Raman spectra of bacteria: a metabolomics profiling by SERS. *Anal. Bioanal. Chem.* **2016**, *408*, 4631–4647.
- (45) Martin, F. L.; Kelly, J. G.; Llabjani, V.; Martin-Hirsch, P. L.; Patel, I. I.; Trevisan, J.; Fullwood, N. J.; Walsh, M. J. Distinguishing cell types or populations based on the computational analysis of their infrared spectra. *Nature protocols* **2010**, *5*, 1748–1760.
- (46) Kjelleberg, S.; Molin, S. Is there a role for quorum sensing signals in bacterial biofilms? *Curr. Opin. Microbiol.* **2002**, *5*, 254–258.
- (47) Orazi, G.; O'Toole, G. A. "It takes a village": mechanisms underlying antimicrobial recalcitrance of polymicrobial biofilms. *J. Bacteriol.* **2019**, 202, No. e00530.
- (48) Prax, M.; Bertram, R. Metabolic aspects of bacterial persisters. Front. Cell. Infect. Microbiol. 2014, 4, 148.
- (49) Bisht, K.; Wakeman, C. A. Discovery and Therapeutic Targeting of Differentiated Biofilm Subpopulations. *Front. Microbiol.* **2019**, *10*, 01908.
- (50) Corbin, B. D.; McLean, R. J.; Aron, G. M. Bacteriophage T4 multiplication in a glucose-limited Escherichia coli biofilm. *Can. J. Microbiol.* **2001**, 47, 680–684.

- (51) Czamara, K.; Majzner, K.; Pacia, M. Z.; Kochan, K.; Kaczor, A.; Baranska, M. Raman spectroscopy of lipids: a review. *J. Raman Spectrosc.* **2015**, *46*, 4–20.
- (52) Middelboe, M.; Jørgensen, N. O. Viral lysis of bacteria: an important source of dissolved amino acids and cell wall compounds. *J. Mar. Biol. Assoc. U. K.* **2006**, *86*, 605–612.
- (53) Vidaver, A. K.; Koski, R.; Van Etten, J. L. Bacteriophage  $\varphi$ 6: a lipid-containing virus of Pseudomonas phaseolicola. *J. Virol.* **1973**, *11*, 799–805
- (54) Sutherland, I. W.; Hughes, K. A.; Skillman, L. C.; Tait, K. The interaction of phage and biofilms. *FEMS Microbiol. Lett.* **2004**, 232, 1–6.

## **□** Recommended by ACS

# **High-Speed Spectral Characterization of Single-Molecule SERS Fluctuations**

Makayla M. Schmidt, Nathan C. Lindquist, et al.

MARCH 23, 2023

ACS NANO

READ 🗹

# Plasmonic-Thermoelectric Nanotweezers for Immersive SERS Mapping

Xianyou Wang, Xiaocong Yuan, et al.

OCTOBER 18, 2022

ACS NANO

READ 🗹

## Nanolaminate Plasmonic Substrates for High-Throughput Living Cell SERS Measurements and Artificial Neural Network Classification of Cellular Drug Responses

Wonil Nam, Wei Zhou, et al.

JULY 26, 2022

ACS APPLIED NANO MATERIALS

READ 🗹

## Characterization of Bacteria Using Surface-Enhanced Raman Spectroscopy (SERS): Influence of Microbiological Factors on the SERS Spectra

Danielle M. Allen, Steven E. J. Bell, et al.

JUNE 17, 2022

ANALYTICAL CHEMISTRY

READ 🗹

Get More Suggestions >